Power-Scale Emulator Design of a DFIG-Based Variable Speed Wind Turbine

J.A. Lopéz-Guevara * **D. del Puerto-Flores** ** **P. Zuniga** **
E. Barocio **

* *Tecnológico Nacional de México, Campus Aguascalientes Aguascalientes, México (e-mail: juan.lg@aguascalientes.tecnm.mx)*
** *Graduate Program in Electrical Engineering, University of Guadalajara (CUCEI), Jalisco, México (e-mail: d.delpuerto,pavel.zuniga,emilio.barocio@academicos.udg.mx)*

Abstract: This work presents the scaled-power emulator design of the doubly-feed induction generator (DFIG)-based variable speed WTS of 1.5 MW, which the power response is scaled to 1.5 kW. The design is composed by a WTS mathematical model, which software-simulated response is used for the configuration of a voltage source converter with LCL filter to act as power source simulating the operation of the WTS model. As a result, software simulation of the proposed scale-power emulator design in a grid-connected scenario is presented, which validated the design, a preliminary stage for a hardware implementation.

Keywords: Scale, Power, Emulator, Design, Wind, Turbines.

1. INTRODUCTION

Nowadays, Wind Power is one of the fastest-growing renewable energy technologies. According to IRENA (2020), global installed wind-generation capacity onshore and offshore has increased in the past two decades, jumping from 7.5 gigawatts GW in 1997 to some 622 GW by 2019. One main issue of the increase is that the wind-turbine capacity has increased over time such that modern's wind power projects have turbine capacities of about 2 MW onshore and $3-5$ MW offshore.

The basic configuration of a Wind Turbine System (WTS) is composed of a mechanical subsystem and an electrical one, where the first subsystem extracts the energy from the wind and makes the wind's kinetic energy available to a rotating shaft; the second subsystem transforms the extracted energy into suitable electrical energy for the electric grid. The two subsystems are connected via the electric generator, an electromechanical system that transforms the mechanical energy into electrical energy, where Synchronous and Induction Generators are the most commonly used and share the actual market, see Ahmed et al. (2020); Teodorescu et al. (2011).

WTS's are based on variable speed generators (VSGs) and fixed-speed generators (FSGs), where key advantages of VSGs compared to FSGs are: they are cost effective and provide simple pitch control; they reduce mechanical stresses; they reduce acoustic noise, because low-speed operation is possible at low power conditions; they improve system efficiency since the operation at the maximum power point (MPP) can be realized over a wide power range; among others. Therefore, direct-in-line VSG systems have been built up to 1.5 MW, and their apparent disadvantages are overcame by an alternative VSG concept that consists of a doubly fed induction generator (DFIG). A WTS based on DFIG allows to reduce inverter cost, because inverter rating is typically 25% of total system power, while the speed range of the VSG is $\pm 33\%$ around the synchronous speed, and power-factor control can be implemented at lower cost, because the DFIG system basically operates similar to a synchronous generator, see Müller et al. (2002).

A typical block diagram of the DFIG wind energy system is shown in Fig. 1, where a wound rotor is fed by a back-to-back system with a rated power of 30% of the generator and the stator is coupled to the grid by a power transformer, see Teodorescu et al. (2011); Ackermann (2005).

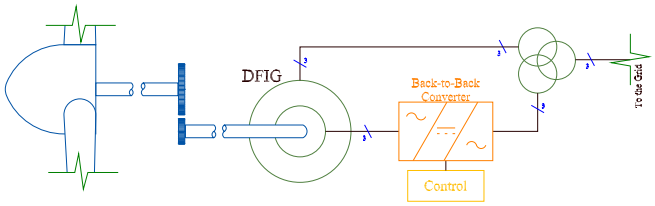

Fig. 1. VSWT scheme with double fed induction generator

For the developing of WTS technologies, adequate environmental conditions are required for testing wind turbines, electrical generators, static power converters and control strategies. Then, emulating the environmental conditions for tests is generally practical and cost-effective. Literature review shows that Wind Turbine System Emulators (WTSE's) rated powers range from few

Watts (e.g. Llano and MacMahon (2017); Ahmed et al. (2016)), some kW (e.g. Gan et al. (2017); Bagh et al. (2012); Camblong et al. (2006)) to MW (e.g. Averous et al. (2017); Muntean et al. (2011)).

WTSE's approach has been used to validate control strategies, Llano and MacMahon (2017); Averous et al. (2017); Muntean et al. (2011), MPP algorithm, Camblong et al. (2006), power electronics applications and hardware-in-the-loop (HIL) technology, Llano and MacMahon (2017); Averous et al. (2017); Muntean et al. (2011) or on repercussions for the generator's mechanical system, Bagh et al. (2012); Gan et al. (2017).

Firstly, WTSEs were developed using direct current (DC) motors as controlled elements to emulate turbines with a coupled alternated current (AC) generators, e.g. Ahmed et al. (2016); Bagh et al. (2012); Camblong et al. (2006), or induction motors, e.g. Gan et al. (2017); Muntean et al. (2011). Later on an alternative approach based on power electronic converters were used to emulate electric machines with "virtual" inertial and damping effect like actual generators, Jiao et al. (2017); Beck and Hesse (2007). In addition, in Huerta et al. (2017) presents the real-time (RT) power-hardware- in-the-loop (PHIL) emulation of the DFIG WT with partial-scale power converter and the PMSM WT with full-scale power converter, where a voltage source converter (VSC) with basic L filter is used as PHIL power interface between the RT simulation and a micro-grid testbed.

This work presents the detailed design of a scaled-power DFIG-based variable speed WTS for a test-bench laboratory implementation. The mathematical models are simulated on Matlab/Simulink environment, which response is used for the configuration of a VSC to act as power sources simulating the operation of WTS model. Moreover, a LCL filter is considered in order to obtain less harmonic distortion of the output power signals.

2. WIND TURBINE SYSTEM MODEL

This section provides dynamic models of wind turbine (WT), Back-to-Back (BTB) Converter, and power flow control schemes.

2.1 Turbine Blade and Rotor Model

The wind power captured by the blade and converted into mechanical power P_m (W) can be calculated by

$$P_m = \frac{1}{2}\rho A v_w^3 C_p(\lambda_T, \beta) \tag{1}$$

where ρ is the air density (=1.225 kg/m^3), A is the sweep area by the blades (m^2), v_w is the wind speed (m/s), and C_p is the power coefficient (of the blade) expressed as a (nonlinear power) function of the tip-speed ratio, λ_T, and the blade angle, β, Wu et al. (2011). However, in Ackermann (2005), for C_p the following equation, to describe the rotor of constant-speed and variable-speed wind turbines, is considered

$$C_p = 0.73\left(\frac{151}{\lambda_i} - 0.58\beta - 0.002\beta^{2.14} - 13.2\right)^{\left(\frac{-18.4}{\lambda_i}\right)} \tag{2}$$

$$\lambda_i = \left[\left(\frac{1}{\lambda_T - 0.02\beta}\right) - \left(\frac{-0.003}{\beta^3 + 1}\right)\right]^{-1} \text{ and } \lambda_T = \frac{\omega_m R}{v_w} \tag{3}$$

where R is the blade radius [m] and ω_m is the WT mechanical speed [rad/s]. Fig. 2 illustrates the variation of C_p for different values of λ_T and β, derived using (2), where the maximum value ($C_{p,\max} = 0.4412$) is obtained for $\beta = 0°$ and $\lambda_T = 7.2$, which is the maximum wind turbine power.

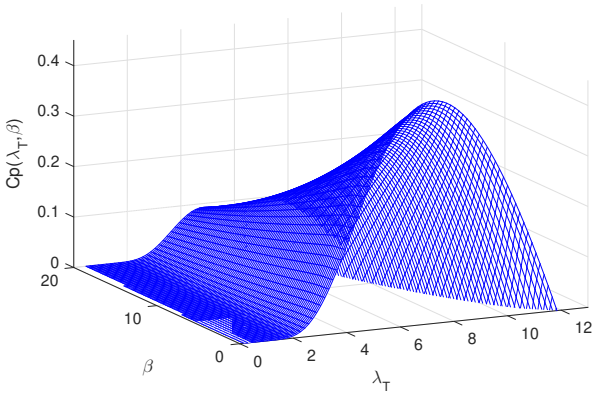

Fig. 2. Power coefficient in function of λ_T and β.

Then, by using per unit (p.u.) system in (1) for different values of v_w, the response is shown in Fig. 3, where the curve $P_{m(\max)}$ represents the trajectory of maximum wind power for different wind velocities. Therefore, for each wind speed, the output power can be maximized by operating at a specific rotational speed.

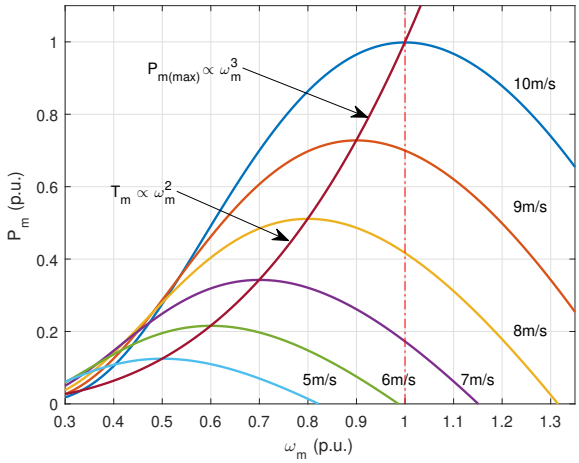

Fig. 3. Mechanical power in function of ω_m.

2.2 Electric Machine Model

A fifth order model of the double fed induction generator (DFIG) is given in the synchronously rotating d-q reference frame, after applying Park transformation, see Ekanayake et al. (2003), by

$$\frac{d}{dt}\lambda_s^d = v_s^d - R_s i_s^d + \omega_s \lambda_s^q \quad (4)$$

$$\frac{d}{dt}\lambda_s^q = v_s^q - R_s i_s^q - \omega_s \lambda_s^d \quad (5)$$

$$\frac{d}{dt}\lambda_r^d = v_r^d - R_r i_r^d + (\omega_s - \omega_r)\lambda_r^q \quad (6)$$

$$\frac{d}{dt}\lambda_r^q = v_r^q - R_r i_r^q - (\omega_s - \omega_r)\lambda_r^d \quad (7)$$

with

$$\lambda_s^d = (L_{l_s} + L_m) i_s^q + L_m i_r^q \quad (8)$$

$$\lambda_s^q = (L_{l_s} + L_m) i_s^d + L_m i_r^d \quad (9)$$

$$\lambda_r^d = L_m i_s^q + (L_{l_r} + L_m) i_r^q \quad (10)$$

$$\lambda_r^q = L_m i_s^d + (L_{l_r} + L_m) i_r^d \quad (11)$$

where, λ are the flux linkages, v and i are the voltages and currents, R, L_l, and L_m are the resistance and self- and mutual-inductances, and ω is the angular velocity, with the subscript r and s for reference variables in the rotor or stator, and superscript d and q for direct and quadrature axis, respectively. Moreover, all the rotor-side parameters and variables are referred to the stator side.

Finally, if T_m is the mechanical torque at the induction generator rotor [Nm], dependent upon the local wind speed, the machine swing equation is given by

$$\dot{\omega}_m = \frac{1}{J}(T_m - T_e), \quad (12)$$

with

$$T_e = \frac{3p_f}{2}\left(i_s^q \lambda_s^d - i_s^d \lambda_s^q\right) \quad \text{and} \quad T_m = \frac{P_m}{\omega_m}, \quad (13)$$

where p_f is the number of machine magnetic pole pairs, T_e is the electromagnetic torque [Nm], ω_m is the rotor mechanical speed, J is the moment of inertial of the rotor machine and the wind turbine [kgm^2], and P_m is the mechanical power from the generator shaft, given by (1).

2.3 Back-to-Back Converter

Fig. 1 shows the WT system of a DFIG connected to the grid through a back-to-back AC/DC/AC converter. Since the power flow through rotor circuit depends on super- and subsynchronous operating modes, the power converter that controls the generator operating point must be bidirectional.

The AC equivalent circuit of the BTB converter is shown in Fig. 4, used to obtain the following dynamic model in a three-phase (abc) stationary reference frame,

$$L_g \frac{d}{dt} i_g = e_g - R_g i_g - v_{cf} \quad (14)$$

$$C_f \frac{d}{dt} v_{cf} = i_g - i_1 \quad (15)$$

$$L_i \frac{d}{dt} i_1 = v_{cf} - R_i i_1 - v_{cd} m_1 \quad (16)$$

$$C_{dc} \frac{d}{dt} v_{dc} = i_1 m_1 - i_2 m_2 \quad (17)$$

$$L_r \frac{d}{dt} i_r = v_{dc} m_2 - v_r \quad (18)$$

where $i_g = [i_g^a, i_g^b, i_g^c]$ and $i_i = [i_i^a, i_i^b, i_i^c]$ are the phase-currents of the grid-side and the converter-side loops, respectively, v_{cf} is the filter capacitor voltage, C_{dc} is the DC-link capacitance, $R_{g,i,r}$ and $L_{g,i,r}$ are the resistances and the inductances of the line(s) used to interconnect the

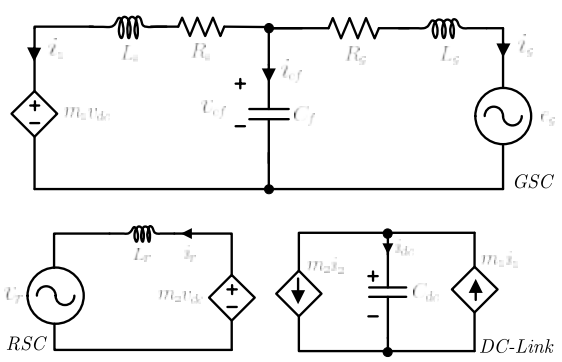

Fig. 4. Model state of BTB Converter equivalent circuit. Upper circuit for GSC with LCL filter, lower-right circuit for DC-link, and lower-left circuit for RSC

BTB converter to the AC systems, v_r is the rotor voltage, and m_1 and m_2 are the modulating signals with the constraints $|m_{1,2}| \leq 1$, Rosas et al. (2009). In addition, e_g is the grid voltage, an infinite bus voltage with neglected Thevenin equivalent line-impedance.

Grid-Side Converter (GSC) control scheme. This control scheme has two main control tasks, one is to track the currents through LCL filter to given current references and the other one is to regulate the DC-link voltage level constant. Therefore, inner and outer control loops are used. By using d–q transformation in (14)-(18), to cancel the nonlinear expressions is used the inner-loop control law:

$$m_1^d = \frac{\omega_1 L_i}{v_{dc}} i_1^q + \frac{v_{cf}^d}{v_{dc}} + k_p(i_1^{d*} - i_1^d) + k_i \int (i_1^{d*} - i_1^d) dt, \quad (19)$$

$$m_1^q = -\frac{\omega_1 L_i}{v_{dc}} i_1^d + k_p(i_1^{q*} - i_1^q) + k_i \int (i_1^{q*} - i_1^q) dt. \quad (20)$$

The outer-loop control law, used to regulate the dc-link voltage level constant, is

$$i_1^{d*} = k_p(v_{dc}^* - v_{dc}) + k_i \int (v_{dc}^* - v_{dc}), \quad (21)$$

where k_p and k_i are proportional and integral constant for each control loop and i_1^{d*}, i_1^{q*}, and v_{dc}^* are the current and voltage references, respectively. Fig. 5 shows the control scheme block diagram, i.e. (19)-(21), for GSC. Notice that the d–q transformation simplifies the tracking control problem of sinusoidal signals to the regulation task of DC values.

Rotor-Side Converter (RSC) control scheme. This control scheme must to keep the wind turbine operating in a given point, typically determined by the maximum power point, and the control law is given by

$$m_2^d = -\frac{(\omega_s - \omega_r) L_r}{v_{dc}} i_r^q + k_p(i_r^{d*} - i_r^d) + k_i \int (i_r^{d*} - i_r^d) dt \quad (22)$$

$$m_2^q = \frac{(\omega_s - \omega_r) L_r}{v_{dc}} i_r^d + k_p(i_r^{q*} - i_r^q) + k_i \int (i_r^{q*} - i_r^q) dt \quad (23)$$

where k_p and k_i are proportional and integral constant and the reference values i_d^* and i_q^* are determined by the

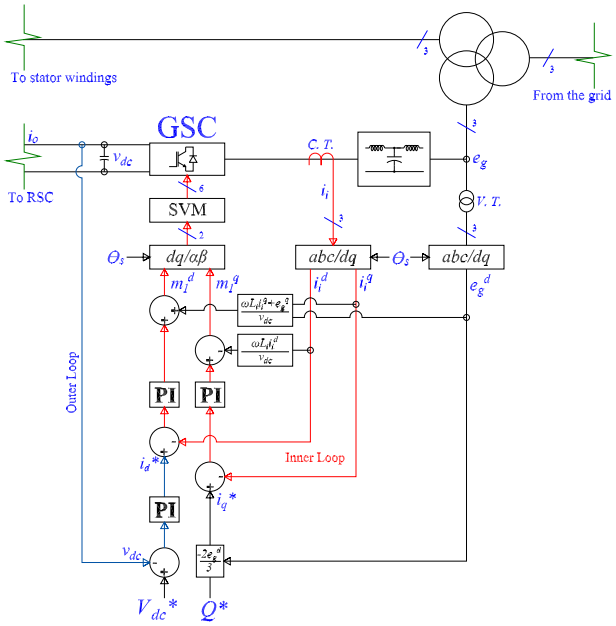

Fig. 5. GSC control scheme block diagram.

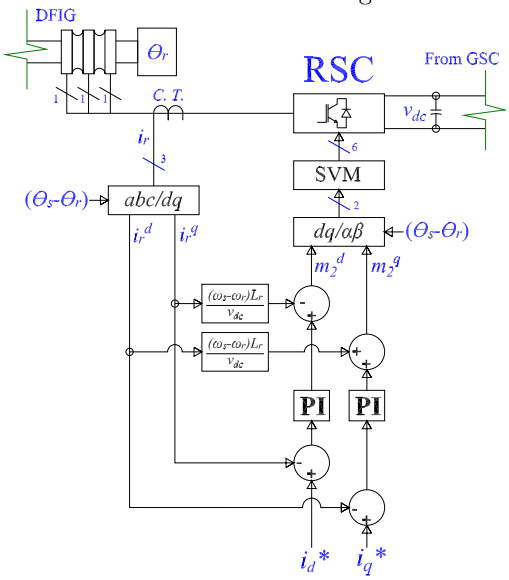

Fig. 6. RSC control scheme block diagram.

desired operating point of power, see Subsection 2.1. Fig. 6 shows the considered control scheme.

3. SCALE-POWER WTS EMULATOR DESIGN

The scale-power WTS emulator is formed by two main stages, firstly via software the WTS mathematical model, previously introduced, is used to determine the emulator operation and, secondly, some output signals of the mathematical models are used as reference signals of the power electronic converters to virtual hardware emulate physical electrical signals, see Fig 7.

3.1 WT mathematical model

Here, we consider the full-scale 1.5 MW WT parameters in Table 1 given in Wu et al. (2011). Since this generator is

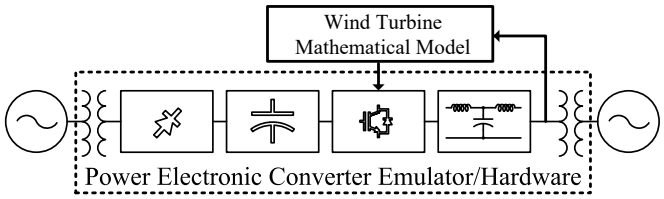

Fig. 7. Block diagram emulador.

Table 1. DFIG 1.5 MW parameters

Parameter	Value	Units
Rated mechanical power P_m	1.5	[MW]
Rated stator phase voltage V_s	398.4	[V] (rms)
Rated rotor phase voltage V_r	67.97	[V] (rms)
Frequency f	50	[Hz]
Rated rotor speed n_g	1750	[rpm]
Rated slip s	-0.1667	
Number of pole pairs p_f	2	
Rated mechanical torque T_m	8.185	[kN·m]
Stator winding resitance R_s	6.25	[mΩ]
Rotor winding resistance R_r	2.63	[mΩ]
Stator leakage inductance L_{ls}	0.1687	[mH]
Rotor leakage inductance L_{lr}	0.1337	[mH]
Magnetizing inductance L_m	5.4749	[mH]

designed to operate in 50 Hz system, it is re-dimensioned into 60 Hz system. Then, we have

$$\omega_{m(60\,\mathrm{Hz})} = (1-s)\frac{2\pi f}{p_f} = 219.9178 \text{ rad/s}, \quad \text{and}$$

$$T_{m(60\,\mathrm{Hz})} = \frac{P_m}{\omega_{m(60\,\mathrm{Hz})}} = 6820.7313 \text{ N·m}.$$

The blade longitude is determined from (1) to produce the nominal mechanical power P_m at a wind speed $v_w = 10\,\mathrm{m/s}$, i.e.,

$$A = \pi r_T^2 = \frac{2P_m}{\rho \cdot v_w^3 C_p} = 5550.7244 \text{ m}^2,$$

therefore, the blade longitude is $r_T = 42.09\,\mathrm{m}$. For this longitude the turbine speed is

$$\omega_T = \frac{\lambda_T \cdot v_w}{r_T} = 1.716\,\mathrm{rad/s} \quad (16.37\,\mathrm{rpm}).$$

For previous rated speed of the generator and turbine, the gearbox ratio r_{gb} is determined as

$$r_{gb} = \frac{(1-s)\cdot 60 \cdot f}{p_f \cdot n_T} = 128.2871.$$

Grid Filter LCL Design. For the BTB converter, the LCL filter inductances must allow to transfer at least 30% of the generator nominal power, normally BTB converter operates around 25% of the stator nominal power of the rotor circuit, therefore a small safety margin is stablished. Moreover, since a current control loop is used in the GSC, the C_f capacitor's influence can be neglected, therefore the filter inductances are considered in series connection and the maximum equivalent inductance is derived by

$$L_{eq(\max)} = \frac{3\sqrt{3}}{2}\frac{(E_g^d)^2}{\omega_s P_e} = 141.63\ \mu\mathrm{H}. \qquad (24)$$

where E_g^d is the grid rms voltage and, using (24) in the procedure from Liserre et al. (2005), the values for the LCL filter are obtained, see Table 2.

Table 2. LCL filter values for GSC of BTBC

Parameter	Value	Units
Rated electric power P_e	450	[kW]
Inverter side inductance L_i	60	[μH]
Grid side inductance L_g	70	[μH]
Capacitance C_f	1000	[μF]
Damping resistance R_d	60	[mΩ]
Resonant frequency f_{res}	885.46	[Hz]
Switching frequency f_{con}	2	[kHz]
Sampling frequency f_s	2	[kHz]

Frequency-Domain Performance Values. The PI controllers are tuned by using the procedure in Teodorescu et al. (2011), where the control systems present the performance summarized in Table 3.

Table 3. BTBC syntonization parameters

	RSC	DC	GSC
Gain margin m_g	∞	∞	8.61 dB
Frequency at m_g, f_{m_g}	∞	∞	641.78 [Hz]
Phase margin m_f	36.84°	39.20°	35.89°
Frequency at m_f, f_{m_f}	107.39 [Hz]	18.12 [Hz]	119.54[Hz]
Bandwidth f_{bw}	181.97 [Hz]	28.65 [Hz]	208.37 [Hz]
Proportional gain k_p	0.2	80	0.1
Integral time T_i	2.9 [ms]	8.7 [ms]	2.9 [ms]

Finally, the WT mathematical model response of Fig. 8 is applied to the "virtual" hardware emulator, namely, a voltage source converter, as power reference values that are injected to the grid, see Fig. 7. In addition, MPPT and Control System blocks can be used to validate different control strategies.

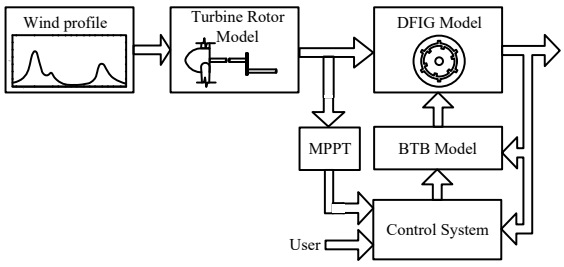

Fig. 8. Wind turbine mathematical model.

3.2 Scale-power WT design

Fig. 7 shows the emulator block diagram, this can be seen as the GSC without considering the DC-link regulation, therefore the control laws (19) and (20) are considered and tuned as the GSC of Subsection 2.3.1. Similar to the LCL filter of BTB converter, the maximum inductance for the LCL filter that guarantees the power transfer is obtained. The nominal electrical power of the emulator is scaled with the ration factor 1000:1, namely, the generator nominal power is 1.5 MW, while the emulator nominal power is 1.5 kW. Table 4 summarizes the control systems and filter parameters, together with the desired performance parameters of the scale-power emulator (SPE).

Table 4. SPE's parameters and performance

Parameter	Value	Parameter	Value
Rated elec. pow. P_e	1.5 [kW]	Gain margin m_g	9.68 [dB]
Inverter side ind. L_i	1 [μH]	Freq. at m_g, f_{m_g}	1387.2 [Hz]
Grid side ind. L_g	2 [μH]	Phase margin m_f	35°
Capacitor C_f	1100 [μF]	Freq. at m_f, f_{m_f}	250.1 [Hz]
Resonant freq. f_{res}	1.95 [kHz]	Bandwidth f_{bw}	433.8 [Hz]
Switching freq. f_{con}	4 [kHz]	Prop. gain k_p	4.9
Sampling freq. f_s	4 [kHz]	Integral time T_i	1.4 [ms]

The control system of the emulator is designed to have a performance with a bandwidth greater that the reference system bandwidth, in order to guarantee that the emulator can reproduce the involving dynamics. Moreover, the gain and phase margins are selected to give a margin for changing of the controller parameters in the emulator implementation due to the considerations done for the WT ideal model.

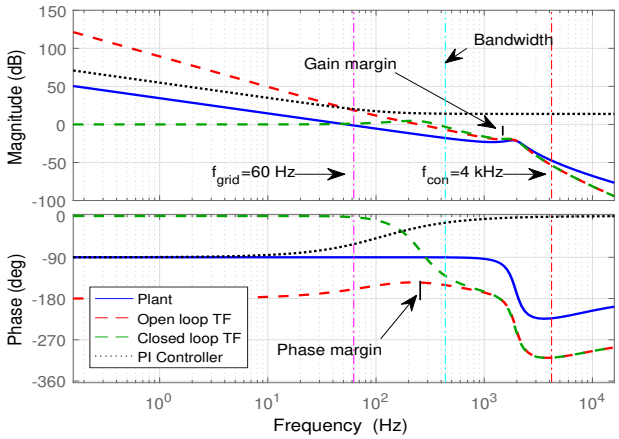

Fig. 9. Emulator bode diagram.

To evaluate the reference signals tracking, the emulator bandwidth is shown in Fig. 9, where the dotted red and green lines are the frequency response for the open and close loop transfer function, respectively, and the solid blue line is frequency response of the emulator's LCL filter.

4. SIMULATION RESULTS

Results from numerical simulation of the DFIG-based WT system with the parameters given in Table 4 and with controllers designed in previous sections are presented here. The simulation results validate the virtual (hardware) emulator, and give better insight into the dynamic operation for a future test-bench laboratory implementation. Therefore, the wind profile, scale-power WT system, and virtual emulator are modeled and simulated using the graphical programming environment Matlab/Simulink.
The power signal generated by the WT mathematical model operating under a given wind profile is applied as reference signal P_{ref}^* (solid red line) to the Virtual Emulator (VE) whose response is plotted as power signal P_{emul} (doted blue line) in Fig. 10. Figure inside Fig. 10 is a zoom in on the power signals, where it shows that the VE's power signal follows the time stochastic variations

of the WT mathematical model power response and the difference between magnitudes is lees that 0.004 p.u.

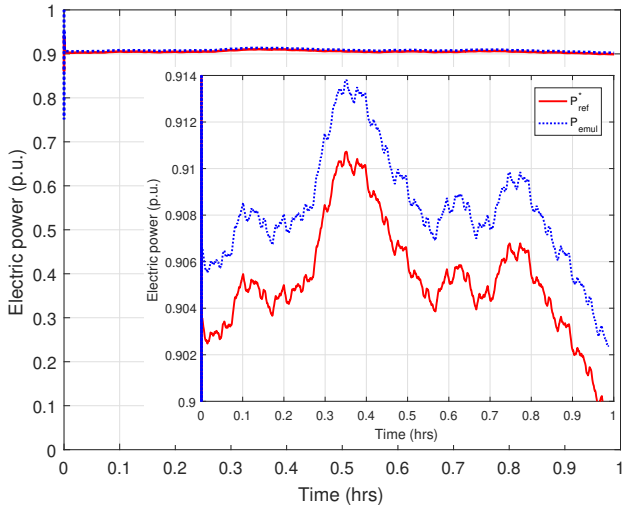

Fig. 10. Scale-Power WT model and HV emulador responses.

Figure 11 shows the transient process of DFIG-based WT (reflects on $|P_s|$) caused by the ramp changes in wind speed, from subsynchronous operation mode v_w, in which the generator operates below the synchronous speed ω_s, to supersynchronous operation mode, above ω_s.

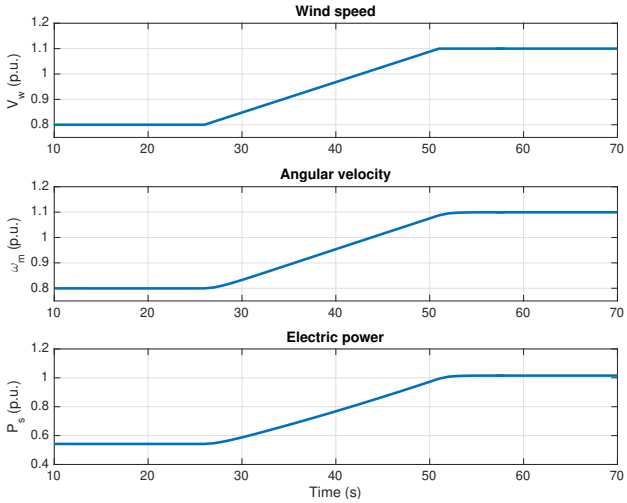

Fig. 11. Transients of DFIG-based WT

REFERENCES

IRENA, *Wind Energy Data*,[Accessed: June 15 2020], Available: http://www.irena.org/wind

S.D. Ahmed, F.S.M. Al-Ismail, M. Shafiullah, F.A. Al-Sulaiman, and I.M. El-Amin, Grid Integration Challenges of Wind Energy: A Review, *IEEE Access*, vol. 8, pp. 10857-10878, 2020.

R. Teodorescu, M. Liserre, and P. Rodriguez, *Grid converters for photovoltaic and wind power system*, Jhon Wiley & Sons, Ltd., 2011.

S. Müller, M. Deicke, and R.W. De Doncker, Double fed induction generator systems for wind turbines, *IEEE Industry Applications Magazine*, May/June 2002.

T. Ackermann, *Wind power in power systems*, John Wiley & Sons Ltd., England, 2005.

B. Wu, Y. Lang, N. Zargari, and S. Kouro *Power conversion and control of energy systems*, Jhon Wiley & Sons, Ltd., England, 2011.

D.X. Llano and R.A. McMahon, *Control techniques with system efficiency comparison for micro-wind turbines*, IEEE Trans. Sustain. Energy, vol. 8, no. 4, pp. 1609-1617, Oct. 2017

C.M. Ahmed, S.J. Plathottam, and H. Salehfar, *Sub kW wind turbine emulator (WTE)*, IEEE Int. conf. on electro information technology, 2016.

L.K. Gan, J.K.H. Shek, and M.A. Mueller, *Modeling and characterization of downwind tower shadow effects using a wind turbine emulator*, IEEE Trans. Ind. Electron., vol. 64, no. 9, 2017.

S.K. Bagh, P. Samuel, R. Sharma, and S. Banerjee, *Emulation of static and dynamic characteristics of a wind turbine using Matlab/Simulink*, 2nd Int. Conf. on Power, Control and embedded Systems, 2012.

H. Camblong, I.M. de Alegria, M. Rodriguez, and G. Abad, *Experimental evaluation of wind turbines maximum power point tracking controllers*, Energy Conversion Management, vol. 47, 2006.

N.R. Averous, M. Stieneker, S. Kock, C. Andrei, A. Helmedag, R.W. De Doncker, K. Hameyer, G. Jacobs, and A. Monti, *Development of a 4MW full-size wind turbine test bench*, IEEE Trans. Emerg. Sel. Topics Power Electron., vol. 5, no. 2, 2017.

N. Muntean, D. Petrila, and O. Pelan, *Hardware in the loop wind turbine emulator*, Int. AEGEAN conf. on electrical machines and power electronics and electromotion, 2011.

Y. Jiao, H. Nian, and G. He, *Control strategy based on virtual synchonous generator under unbalanced grid voltage*, 2017 20th Int. Conf. on electrical machines and systems, pp. 1–6, 2017.

H. P. Beck and R. Hesse, *Virtual synchronous machine*, 2007 9th Int. Conf. on electrical power quality and utilisation, pp. 1-6, 2007.

F. Huerta, R.L. Tello, and M. Prodanovic, *Real-Time Power-Hardware-in-the-Loop Implementation of Variable-Speed Wind Turbines*, IEEE Trans. Ind. Electron., vol. 64, no. 3, pp. 1893-1904, 2017.

J.B. Ekanayake, L. Holdsworth, and N. Jenkins, *Comparison of 5th order and 3rd order machine models for dubly fed induction generator (DFIG) wind turbines*, Electric Power Systems Research, pp. 207–215, 2003.

E. Rosas, V. Cárdenas, J. Alcalá, and C. Nuñez, *Active and reactive current decoupled control strategy applied to a single-phase BTB converter*, Int. conf. on electrical eng., computating science & automatic control, 2009.

M. Liserre, F. Blaabjerg, and S. Hansen, *Design and Control of an LCL-Filter-Based Three-Phase Active Rectifier*, IEEE Trans. Ind. Appl., Vol. 41, pp. 1281-1291, no. 5, 2005.

